Hindawi
Advances in Civil Engineering
Volume 2019, Article ID 7419752, 11 pages
https://doi.org/10.1155/2019/7419752

Research Article

Experimental Investigation of Energy Evolution in Sandstone Failure during Triaxial Unloading Confining Pressure Tests

Rui Yang,[1,2] Depeng Ma ,[3] and Yongjie Yang[4]

[1]*State Key Laboratory for Geomechanics and Deep Underground Engineering, China University of Mining and Technology, Xuzhou 221116, China*
[2]*School of Mechanics and Civil Engineering, China University of Mining and Technology, Xuzhou 221116, China*
[3]*College of Water Conservancy and Civil Engineering, Shandong Agricultural University, Tai'an 271018, China*
[4]*College of Mining and Safety Engineering, Shandong University of Science and Technology, Qingdao 266590, China*

Correspondence should be addressed to Depeng Ma; yr950726@yeah.net

Received 26 December 2018; Revised 2 March 2019; Accepted 9 April 2019; Published 2 May 2019

Academic Editor: Pier Paolo Rossi

The deformation and failure of sandstone samples are closely related to energy changes in the material. To explore the energy evolution during the process of sandstone sample damage, loading and unloading tests with different test paths were conducted. The results show that more energy is stored and consumed before the stress reaches its peak, while after the peak stress, more energy is released and consumed. Energy dissipation increases internal cracking, leads to sample damage and lithologic deterioration, and reduces the bearing capacity of the sample. During triaxial unloading of the confining pressure, the higher the initial unloading confining pressure, the more the elastic energy stored, and the more the energy released when the sandstone sample fails, resulting in more severe damage. Therefore, during the excavation of high-stress rock masses, large amounts of elastic energy stored in sandstone can be rapidly released, leading to rock burst disasters. Additionally, during triaxial unloading confining pressure tests, the damage in sandstone when the sample is close to failure increases more rapidly than that during conventional triaxial compression tests because of the unloading effect of the confining pressure. This phenomenon also illustrates that the failure of sandstone induced by unloading is more sudden than that induced by loading.

1. Introduction

Mining, tunnel excavation, and other projects in deep mines involve high-stress rock unloading, which often leads to serious accidents that threaten the security of mining [1]. From a thermodynamic point of view, the failure process of a rock mass is seen as a state of energy-driven instability, and the deformation and failure of the rock mass are directly related to its energy conversion. Therefore, by focusing on the energy conversions during the processes of rock deformation and damage, the essential characteristics of rock failure can be further revealed.

By analyzing the evolution of energy in the material, valuable numerical results about the failure regularity of rock have been acquired. Lan et al. [2] studied the distribution of elastic energy within a rock mass by analyzing the tectonic stress field distribution and obtained the stress and energy conditions at the time of rock burst. Cong et al. [3] and Yang et al. [4] performed conventional compression tests on marble specimens to analyze the changes in energy during the failure of the specimens. Based on experimental results, Liu et al. [5] analyzed the relationship between the energy and the strain in marble under loading and unloading. Based on conventional triaxial compression tests and unloading confining pressure tests of brittle granite under different experimental conditions, Chen et al. [6] obtained a criterion for rock burst based on energy principles. Chen et al. [7] revealed the characteristics of energy changes in marble under high confining pressure triaxial unloading tests. Zhao et al. [8] built the connection between the acoustic emission energy and the efficiency of rock failure under the combined action of dynamic and static

loads on granite. Huang et al. [9] analyzed the energy evolution mechanism of coarse-grained marble under uniaxial compression. Pan et al. [10] presented comprehensive stiffness and comprehensive energy criteria for rock failure. Song and Yang [11] performed uniaxial compression tests of coal rock to examine the energy evolution of coal pillar failure. Zhang et al. [12] studied energy dissipation during tensile failure of saturated water samples. Based on uniaxial compression and triaxial compression tests, Ma et al. [13] studied the influence of the loading rate and confining pressure on the energy dissipation characteristics of coal samples. In addition, many scholars have studied the mechanical and acoustic emission characteristics of sandstone under different stress paths [14–19].

These results provide important references for the study of rock energy evolution and the relationship between rock energy evolution and rock deformation and failure. However, these studies mainly examined marble and granite under uniaxial compression, conventional triaxial compression, and triaxial unloading and confining pressure. In addition, a number of studies have investigated energy evolution in sandstone with certain conventional test paths, such as uniaxial compression and triaxial compression, but research on energy conversions during triaxial unloading confining pressure tests in sandstone is scarce.

To explore the essential characteristics of sandstone deformation and failure, we performed triaxial compression and triaxial unloading tests of sandstone under different confining pressures and studied the energy changes during the damage process under triaxial compression and triaxial unloading confining pressure. The results may be used as guidance for the prevention and control of mine disasters caused by excavation and stress unloading in deep mines.

2. Materials and Methods

2.1. Sample Selection. Samples of test rock were taken from the roof sandstone of the No. 3 coal in Yangcun Coal Mine, Jining, Shandong, China. According to the engineering rock mass test standards, the coal block was cut into 50×100 mm (diameter × height) cylinders. To ensure that the specimens were similar and homogeneous, they were subjected to ultrasonic testing, and the specimens that showed high wave velocities were removed, leaving the specimens with similar velocities. The rock samples used in the test are shown in Figure 1.

2.2. Test Program. Triaxial loading and unloading tests were carried out on the MTS815.02 electrohydraulic servo rock mechanics test system of the China University of Mining and Technology. The test system could meet the test requirements under a variety of complex paths. The test plan in this study was as follows:

Loading tests: triaxial tests of specimens under different confining pressures were carried out; the confining pressure (4 MPa, 7 MPa, or 10 MPa) was gradually applied under hydrostatic pressure. Under constant confining pressure, the axial pressure was increased by axial displacement control at a loading rate of 0.002 mm/s until the specimen failed.

Triaxial unloading confining pressure tests: during the process of mining, the lateral stress in coal bodies (equivalent to the confining pressure) is gradually reduced, and the advanced support pressure (equivalent to the axial stress) is gradually increased. Working face mining is actually the process of reducing the confining pressure and increasing the axial pressure of the rock mass and its surroundings.

Therefore, the experiment adopted the loading path of increasing axial pressure and decreasing confining pressure. Under this path, the failure of the specimen is quickest and most dangerous. The experiment was divided into three stages: (1) increase the confining pressure (σ_3) gradually to a predetermined value (4 MPa, 7 MPa, or 10 MPa) according to the hydrostatic pressure condition; (2) keep the value of σ_3 unchanged and increase the axial pressure (σ_1) to eighty percent of the peak compressive stress from conventional triaxial tests through the stress control method; and (3) use the displacement control method to increase the value of σ_1, and at the same time, decrease the value of σ_3 at a rate of 0.05 MPa/s until the specimen is destroyed. Then, the decreasing of the confining pressure is stopped immediately after the specimen is damaged, while the axial pressure continues to load to the residual strength of the specimen using the displacement control method. The stress path of the unloading confining pressure is shown in Figure 2, and the test process and posttest sample are shown in Figure 3.

3. Energy Calculation Principles

When conventional triaxial compression tests or confining pressure triaxial unloading tests are carried out, the specimen is placed in the triaxial chamber of the testing machine, and the specimen and the testing machine are regarded as a closed system. Thus, during the deformation, damage, and destruction of the specimen in the triaxial chamber, no energy is exchanged with the outside environment, and energy exchange occurs solely within the testing apparatus.

In conventional triaxial compression tests, in addition to the axial energy U_1 produced by the testing machine, the machine also produces and maintains the hydrostatic pressure, which also does positive work on the specimen (U_0). After the hydrostatic pressure stage, the axial pressure continues to increase, and the axial force applied to the specimen is constantly positive. As the axial force increases, the radial deformation of the cylindrical specimen increases, which causes the confining pressure to perform negative work [20], which is denoted as U_3. The total energy of the rock sample during the triaxial compression test is as follows:

$$U = U_1 + U_3 + U_0. \tag{1}$$

Furthermore, the total energy U is converted into two energies: the elastic energy U_e stored in sandstone that can be released when the specimen fails and the dissipation energy U_d that is consumed by internal crack expansion,

(a) (b)

Figure 1: Processing of rock samples.

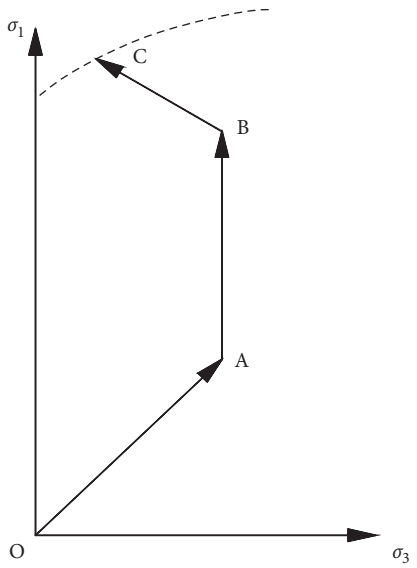

Figure 2: Stress path of unloading confining pressure.

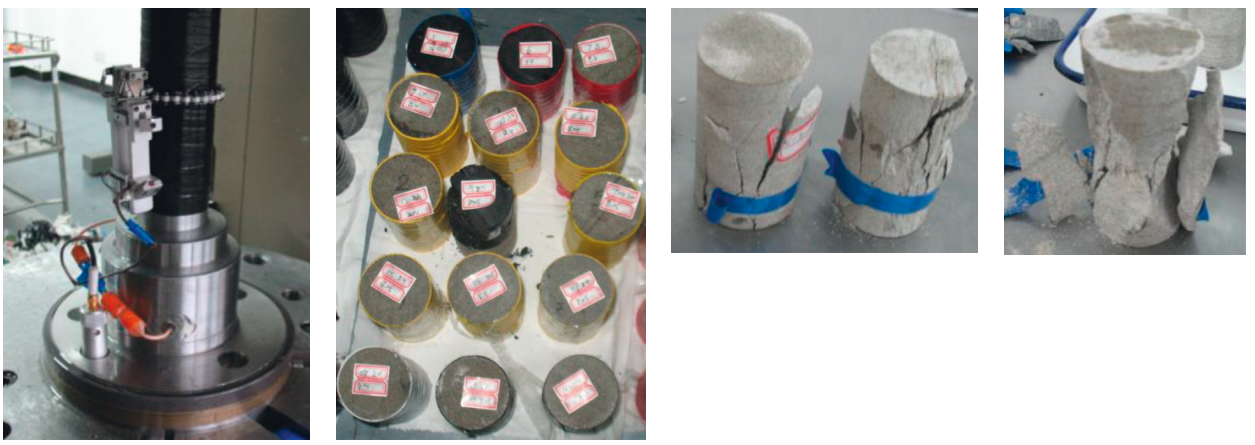

(a) (b) (c) (d)

Figure 3: Test process and rock samples after testing.

friction, and other processes during the damage of the specimen. This relation can be expressed as follows:

$$U = U_d + U_e. \tag{2}$$

Combining formulas (1) and (2), we obtain

$$U_1 + U_3 + U_0 = U_d + U_e. \tag{3}$$

The loading path of the triaxial unloading confining pressure tests lies between those of the uniaxial compression tests and the conventional triaxial compression tests. When the unloading rate of the confining pressure is relatively fast, the confining pressure decreases to 0 rapidly, which is similar to a uniaxial stress state. When the unloading rate of the confining pressure is relatively slow, the confining pressure decreases by a very small value for a period of time, which is similar to a conventional triaxial test. Therefore, the principle of energy calculation in the conventional triaxial test is also applicable to triaxial unloading confining pressure tests.

The calculation methods of the above energy [21–23] are as follows:

(1) The energy of the hydrostatic stress state (U_0) can be calculated directly from the formulas related to elasticity:

$$U_0 = \frac{3}{2}\frac{1-2\mu}{E}\sigma_3^2. \tag{4}$$

(2) The axial energy (U_1) and the energy consumed by negative work under the confining pressure (U_3) can be calculated by the integral method according to the stress-strain curve:

$$U_1 = \int \sigma_1 d\varepsilon_1 = \sum_{i=0}^{n} \frac{1}{2}\left(\varepsilon_1^{i+1} - \varepsilon_1^{i}\right)\left(\sigma_1^{i} + \sigma_1^{i+1}\right), \tag{5}$$

$$U_3 = 2\int \sigma_3 d\varepsilon_3 = \sum_{i=0}^{n}\left(\varepsilon_3^{i+1} - \varepsilon_3^{i}\right)\left(\sigma_3^{i} + \sigma_3^{i+1}\right). \tag{6}$$

In these formulas, σ_1^i and σ_3^i are the axial stress and confining pressure corresponding to a certain point, and ε_1^i and ε_3^i are the axial strain and circumferential strain corresponding to a certain point, respectively.

(3) At a certain time t, the elastic energy (U_e) stored in a rock sample can be calculated by the following formula:

$$U_e = \frac{1}{2E_i}\left[\sigma_1^2 + 2\sigma_3^2 - 2\mu_i\left(2\sigma_1\sigma_3 + \sigma_3^2\right)\right], \tag{7}$$

where E_i and μ_i are the modulus of elasticity and Poisson's ratio at a certain point, respectively.

(4) Formula (2) can be rewritten as follows, which can be adopted to define the dissipation energy (U_d):

$$U_d = U - U_e. \tag{8}$$

According to formulas (1)–(8), we compiled a corresponding program to calculate the energy of each sample, and the calculation results were analyzed. In addition, we should explain that the energy calculated by formulas (1)–(8) is essentially the energy density of each energy index.

4. Energy Evolution Characteristics of Sandstone under Different Experimental Paths

According to the stress-strain curve obtained from the experimental results, the energy of the sandstone under different test conditions is calculated using the energy calculation methods described in this paper. The results are plotted in certain curves to analyze the characteristics of energy evolution.

4.1. Energy Evolution Characteristics of the Loading Test. Figure 4 shows the stress-strain curve (black line) and the evolution of the various energies (colored lines) in the specimen as the axial strain ε_1 increases under a confining pressure of 10 MPa. The hydrostatic energy in the triaxial compression test is accumulated in the specimen during hydrostatic loading. Therefore, all the energy curves in the figure originate from the same point (the hydrostatic pressure), and the curves describe the energy evolution after the hydrostatic loading stage.

At the beginning of the test, U_3 shows little change, and U_d increases slightly. U_1, U_e, and U increase with the axial strain, and they are almost indistinguishable. The results show that although energy dissipation occurs during the compaction stage when the sandstone displays the behavior of crack closure, the consumption is very low.

Then, the sample is in the elastic stage (between dashed lines A and B), and as the axial force increases, U_1 rises at an increasing rate. The concave curve of U_1 indicates that although the natural cracks in the sandstone are narrow and closed in the compaction stage, new cracks appear in the sandstone as the axial stress increases, and the appearance and extension of the new cracks consume some energy. Therefore, U_d increases at this stage. At the same time, U_3 increases with the axial force, indicating that the radial strain in the sandstone sample also increases. At this stage, the trends of U_e and U are still similar to that of U_1, but the difference between U_1 and U_e increases as a result of the increase in U_d and U_3.

After the sandstone enters the plastic deformation stage (between points B and C), U_1 increases at a high rate. As the axial stress continues to increase, certain cracks are generated and developed, resulting in significant deformation by

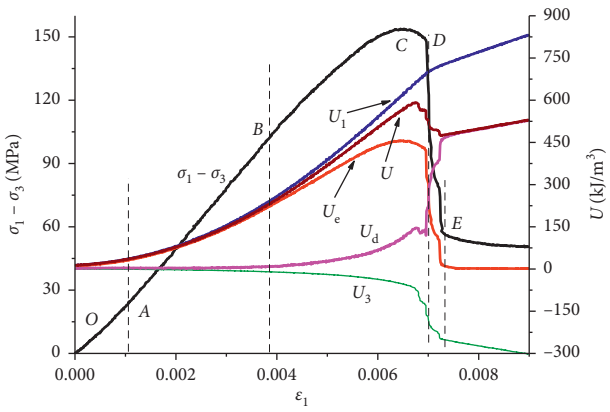

Figure 4: Energy curves of the rock sample under a confining pressure of 10 MPa.

radial dilatancy of the sandstone. In this respect, both U_d and U_3 began to increase rapidly. Near the peak stress, U_e and U continue to grow but at slower rates, while U_d and U_3 increase at higher rates.

When the sandstone reaches the peak stress (point C), the elastic energy U_e is released, while the increase rates of U_d and U_3 show further improvement. In addition, the total energy curve reaches the turning point and begins to decrease, and the differences between U_1, U_e, and U increase gradually.

After point D, the stress-strain curve indicates a rapid release of U_e. The strength of the specimen decreases rapidly, and the sample loses its bearing capacity because of the formation of a macroscopic fracture surface in the sandstone. The increase rate of U_1 also decreases; however, U_d and U_3 increase exponentially within a very short time, whereas U decreases suddenly as the sandstone enters the residual plastic phase.

After point E, U_d and U_3 continue to increase at slower rates. U_e continues to decrease at a slower rate, and U_1 continues to increase at a slower rate. The total energy of the system increases again but also at a slower rate. After a period of intense energy conversion, the energy of the system gradually stabilizes, maintaining a relatively balanced state.

4.2. Energy Evolution during Triaxial Unloading Confining Pressure. During the triaxial unloading confining pressure, the hydrostatic energy also accumulates at the hydrostatic loading stage of the sandstone. Therefore, all the curves originate at the hydrostatic pressure point, and the analysis focuses on the energy evolution after the hydrostatic loading stage. Figure 5 shows the energy evolution of sandstone under a confining pressure of 7 MPa and an unloading pressure rate of 0.05 MPa/s.

At the beginning of the test, both U_3 and U_d show linear increases within short periods of time. U_1, U_e, and U also increase slightly with the loading time and axial strain, and they follow very similar paths. These results illustrate that, during the compaction stage of axial loading, the energy dissipation in the sample is relatively low.

Before the confining pressure is applied, as the axial force increases, U_1 begins to increase gradually at an increasing rate, which produces a concave curve. At this stage, U_d also begins to increase gradually, indicating the occurrence and development of cracks in the sandstone, which results in a certain consumption of energy. As the radial strain of the sandstone specimen increases, U_3 also shows obvious growth. At this stage, the trends of U_e and U are still similar to that of U_1, but the differences between U_1, U_e, and U increase gradually due to the increases in U_d and U_3.

When the confining pressure is applied, U_1 and U_e continue to increase, and U_3 and U_d also increase but at higher rates. However, the supply of energy is still higher than the consumption of energy. Hence, the total energy U increases with a higher growth rate than in the previous stage.

When the peak stress value is reached, a large amount of elastic energy is rapidly released. The cracks in the sandstone converge and form a macroscopic fracture surface. The dissipation energy U_d and the radial strain increase rapidly, resulting in an increase in U_3. Although the axial energy continues to increase at this time, it increases at a slower rate due to the decrease in axial force as a result of the damage to the sandstone. In addition, with the rapid decrease in U_1, the total energy U also decreases sharply, and the energy conversion in this stage is more obvious than that in the previous stages.

After the plastic flow stage, the axial strain continues to increase with time, whereas both energy indexes tend to be stable.

According to the energy-radial-strain curve and the energy-volume-strain curve during the experiment, at the beginning of the test, the rules of energy varying with radial strain and volume strain are similar to the rules of energy varying with time and axial strain, which increases with strain. When the confining pressure is applied, the radial strain increases, and the value of volume strain is negative, indicating dilatancy in the sandstone. At the same time, U_1 continues to grow, while U_d and U_3 show similar linear increases. Since U_d and U_3 reflect the damage and the volume dilation of the samples, respectively, the two processes during the test are indicated to occur simultaneously.

Overall, under the different test paths, such as the conventional triaxial compression test or the triaxial unloading confining pressure test, the energy in sandstone is mainly in the form of storage and dissipation before the peak stress, whereas the energy is mainly in the form of release and dissipation after the peak stress. In addition, energy dissipation expands the internal cracks in the sandstone, which results in damage to the rock and a decrease in the bearing capacity, while energy release causes instability and failure in the sandstone, as shown in Figure 5.

5. Influence of the Unloading Confining Pressure on Energy Evolution

5.1. Relationship between Energy Evolution and Unloading of the Initial Confining Pressure. Figures 6 and 7 present a comparison of the elastic energy curves under different

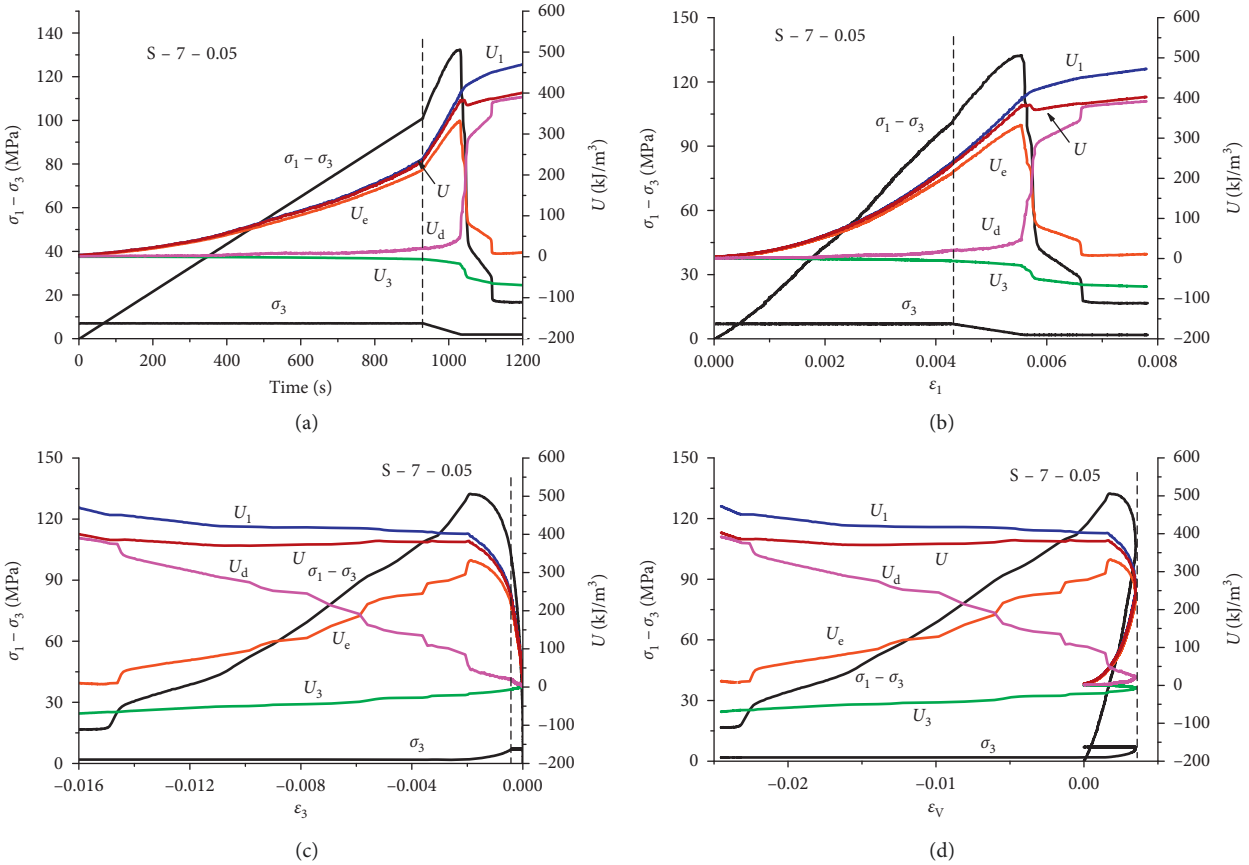

Figure 5: Energy evolution curves of sandstone samples under unloading confining pressure. (a) Energy-time curve (C-7-0.05). (b) Energy-axial-strain curve (C-7-0.05). (c) Energy-radial-strain curve (C-7-0.05). (d) Energy-volume-strain curve (C-7-0.05).

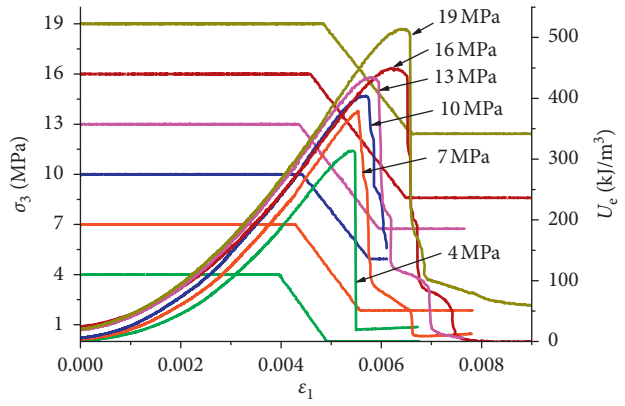

Figure 6: Comparison of elastic energy curves under different confining pressures.

confining pressures and a comparison of the dissipated energy curves under different confining pressures, respectively. The evolution of the elastic energy and dissipated energy under different unloading of the initial confining pressures are as follows.

5.1.1. Evolution of Elastic Energy with Initial Unloading Confining Pressure. At the axial loading stage, the higher the initial unloading confining pressure is, the greater the elastic energy of the sandstone is. The growth rate of elastic energy at high confining pressure is higher than that at low confining pressure. Then, when the confining pressure is unloaded, the elastic energy still increases, but the increase rate decreases with the unloading of the confining pressure. After the peak stress, a large amount of elastic energy is released, and the value of U_1 decreases sharply. Furthermore, the higher the initial confining pressure is, the greater the decrease in U_1, causing a greater release of the elastic energies when the sandstone fails, as shown in Figure 6.

5.1.2. Evolution of Dissipation Energy with Initial Confining Pressure. During the early stages of the test, the dissipation energy increases gradually; however, under different confining pressures, the growth curve changes from linear to nonlinear. Moreover, the higher the confining pressure is, the faster the growth rate is. After the start of the unloading, the dissipation energy increases further. When the stress is near the peak value, the sandstone specimen fails, and dissipation increases sharply. The higher the initial confining pressure is, the greater the dissipation energy is, as shown in Figure 7.

5.2. Relationship between the Energy at Peak Stress and the Initial Confining Pressure. The energy indexes of the

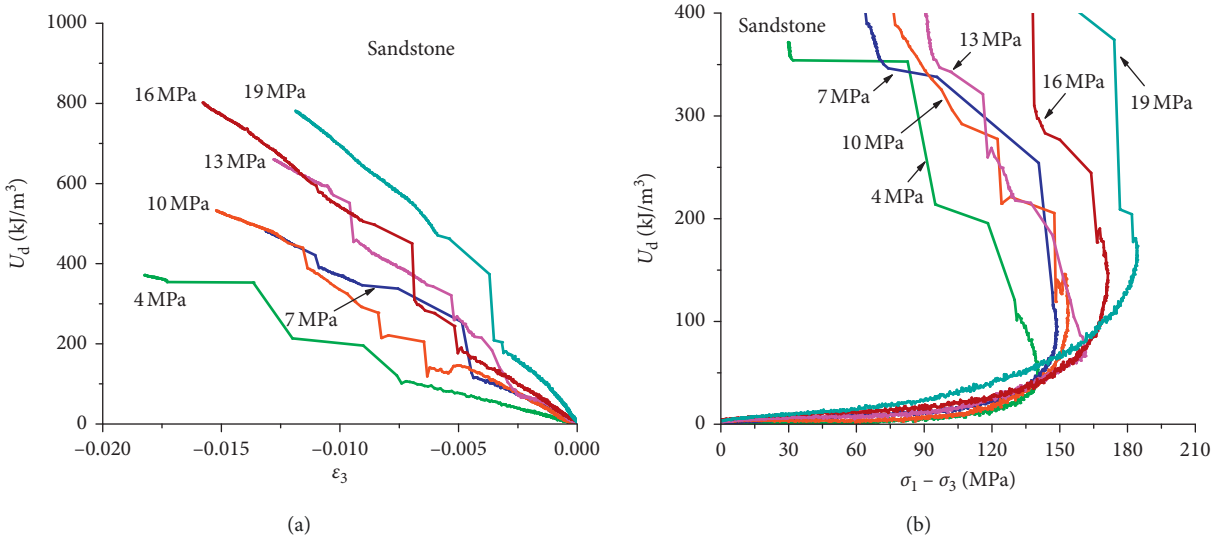

FIGURE 7: Comparison of dissipated energy curves under different confining pressures. (a) Dissipative energy-radial strain curve. (b) Dissipated energy-deviation stress curve.

sandstone at the peak stress under different initial unloading confining pressures are shown in Table 1. Both energy indexes at peak stress are found to increase with the initial unloading confining pressure. During the axial loading stage, the ultimate strength and axial strain of the sandstone increase with initial confining pressure. The time of energy accumulation before the peak stress is also positively correlated with the initial confining pressure; thus, the axial energy, elastic energy, and total energy at the peak stress have similar tendencies. At initial confining pressures of 7, 10, 13, 16, and 19 MPa, the U_1 values are 1.29, 1.59, 1.66, 1.71, and 2.06 times the value when the initial confining pressure is 4 MPa, respectively; the U_e values are 1.31, 1.40, 1.44, 1.48, and 1.75 times, respectively; and the U values are 1.29, 1.50, 1.56, 1.61, and 1.90 times the value when the initial confining pressure is 4 MPa, respectively.

U_3 is the cumulative energy used to overcome the work performed by the confining pressure during the increase in radial deformation. The higher the initial confining pressure, the higher the U_3 increase during the axial loading stage. Similarly, the higher the initial confining pressure is, the greater the limitation on the sandstone specimen at the axial loading stage, and the more energy is consumed during the appearance and development of cracks in the sandstone; thus, U_d increases with the confining pressure. At confining pressures of 7, 10, 13, 16, and 19 MPa, the U_3 values are 4.31, 3.26, 3.65, 3.74, and 5.19 times the value when the confining pressure is 4 MPa, respectively; and the U_d values are 1.76, 2.39, 2.53, 2.70, and 3.12 times the value when the confining pressure is 4 MPa, respectively.

5.3. Characteristics of Energy Conversion during the Unloading Confining Pressure Stage. To accurately reflect the energy characteristics of the sandstone specimens during this stage with different initial unloading pressures, we eliminate the energy of the specimen obtained from the axial loading stage, and the energy difference ΔU between the point where the unloading of the confining pressure starts and the point where the peak stress is defined. At the same time, the conversion rate $V_{\Delta U}$ ($V_{\Delta U} = \Delta U/\Delta t$) is calculated, in which Δt is the time corresponding to ΔU. The energy increment (left axis) and the energy conversion rate (right axis) of the sandstone specimens during the unloading of the different confining pressures are shown in Figure 8.

During the unloading of the confining pressure stage, all the axial energy increments ΔU_1 of the sandstone specimens, the energy dissipation increments ΔU_3, the elastic energy increments ΔU_e, the depletion energy increments ΔU_d, and the total energy increments ΔU increase with initial confining pressure, and the conversion rate of each energy index shows the same behavior. Under an initial confining pressure of 19 MPa, the energy increments ΔU_1, ΔU_3, ΔU_e, ΔU_d, and ΔU of the specimens are 2.07, 4.82, 1.38, 3.32, and 1.49 times their values when the initial confining pressure is 4 MPa, respectively, and the conversion rates are 1.40, 3.26, 0.93, 2.25, and 1.01 times their values when the initial confining pressure is 4 MPa, respectively. These results indicate that the effect of the initial confining pressure on the five energy indexes is different. ΔU_3 shows the largest change among these energy indexes, indicating that the initial unloading confining pressure has a great influence on the radial deformation of the sandstone samples.

5.4. Energy Comparison between the Axial Loading Stage and the Pressure Unloading Stage. Figure 9 shows the energy differences in the sandstone specimens between the axial loading stage (before unloading of the confining pressure) and the unloading stage (the point when the unloading of the confining pressure starts to the point of peak stress) for the different initial unloading confining pressures.

The accumulations of ΔU_e and ΔU in the sandstone samples during the axial loading stage are higher than those

Table 1: Energy levels at peak stress under different initial unloading confining pressures.

Lithology	Initial unloading confining pressure (MPa)	Unloading pressure rate (MPa/s)	$\sigma_1 - \sigma_3$ at peak stress (MPa)	Energy at peak stress (kJ/m^3)				
				U_1	U_3	U_e	U_d	U
Sandstone	4	0.05	129.08	351.01	−16.96	298.70	35.35	334.06
	7	0.05	132.39	452.57	−22.23	368.06	62.28	430.34
	10	0.05	136.94	556.68	−55.36	416.70	84.62	501.32
	13	0.05	145.56	581.67	−61.86	430.23	89.58	519.81
	16	0.05	154.78	599.73	−63.37	440.85	95.50	536.36
	19	0.05	175.7	722.39	−88.05	523.95	110.40	634.35

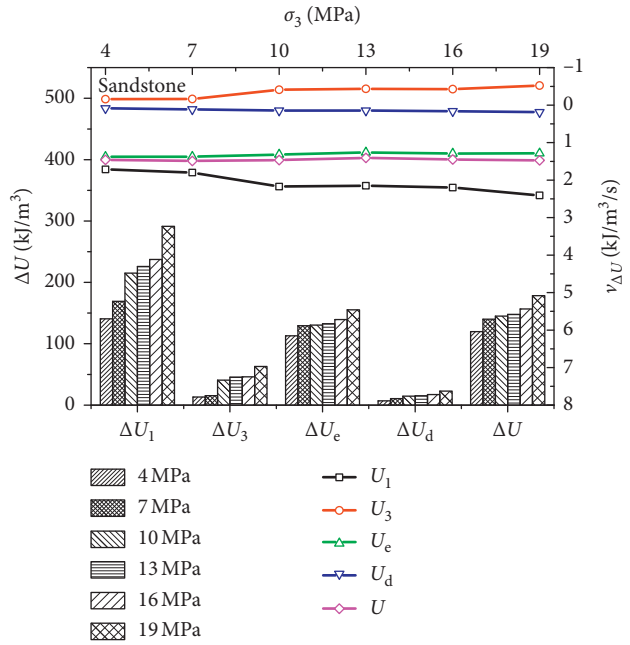

Figure 8: Energy transformation during the unloading of the confining pressure under different initial confining pressures.

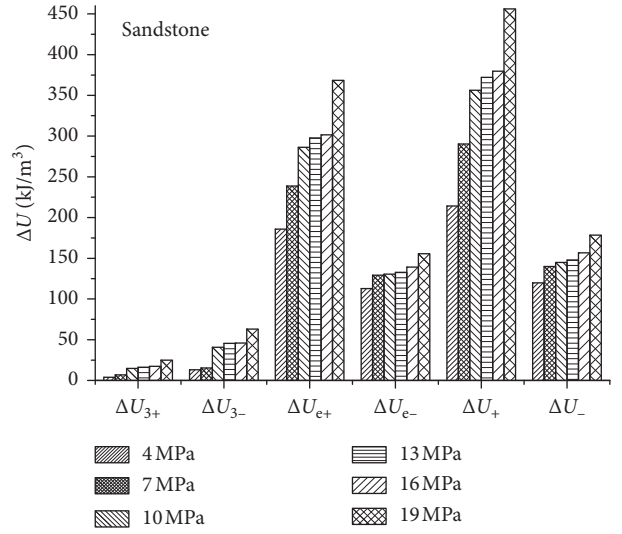

Figure 9: Energy transformation of loading and unloading confining pressure periods under different initial unloading confining pressures.

during the unloading stage. For example, under an initial confining pressure of 7 MPa, ΔU_e and ΔU during the axial loading stage are 47.47 kJ/m^3 and 53.08 kJ/m^3, respectively, whereas they are 20.35 kJ/m^3 and 25.31 kJ/m^3 during the unloading stage, respectively. Thus, the axial loading stage contributes more energy storage in the sandstone samples. In particular, the driving energy (U_e) of sandstone failure reaches 70% during the loading stage, suggesting that the energy accumulation in the axial loading stage plays a major role in sandstone failure. Additionally, the higher the initial confining pressure is, the greater the elastic energy that accumulates during the axial loading stage, which induces the rapid release of U_e, causing more serious disasters.

In practical engineering, the release of elastic energy in rock with high-stress conditions is significantly higher than that in rock under low-stress conditions when the rock fails. Therefore, when a high-stress rock mass is excavated, much elastic energy can be released rapidly, resulting in rock burst and other geological disasters.

Unlike ΔU_e and ΔU, ΔU_3 shows the opposite behavior. During the axial loading stage, the accumulation of U_3 in the sandstone is less than that during the unloading stage. This result indicates that the increase in radial deformation occurs mainly during the unloading stage, and the higher the initial confining pressure is, the higher the U_3 that accumulates during the unloading stage.

6. Analysis of Sandstone Damage Based on Dissipation Energy

6.1. Damage Evolution Model. In this paper, we assume that any external work performed on the sandstone specimens is converted into elastic energy and dissipative energy and that all the dissipation energy contributes to the damage to the sandstone. Hence, during the experiment, the damage caused by different stress paths, such as axial loading and radial unloading, can be regarded as the work of dissipation energy. The more the dissipation energy used, the greater the damage to the sandstone. Therefore, based on the definition of damage by Kachanov [24] and the research of Liu et al. [25] and other studies, the model of rock damage evolution based on the energy transformation principle is obtained as follows:

$$D = \left(1 - \frac{\sigma_C}{\sigma_P}\right) \frac{U_d}{U_{d\max}}, \tag{9}$$

where $U_{d\,max}$ is the value of the dissipation energy when the rock is completely destroyed, U_d is the dissipation energy when the damage area of the section reaches a certain value A_d, σ_P is the peak stress, and σ_C is the residual stress.

According to the elastic mechanics and related references, the constitutive stress-strain relation in the rock considering the damage characteristics can be expressed as

$$\sigma_1 = 2\mu\sigma_3 + E(1-D)\varepsilon_1. \tag{10}$$

Substituting formula (9) into formula (10), we obtain

$$\sigma_1 = 2\mu\sigma_3 + E\left(1-\left(1-\frac{\sigma_C}{\sigma_P}\right)\frac{U_d}{U_{d\,max}}\right)\varepsilon_1. \tag{11}$$

6.2. Energy-Based Damage Characteristics of Sandstone under Triaxial Compression. Based on the test results and formula (11), we calculate the damage curves of sandstone under conventional triaxial loading and triaxial unloading confining pressure tests, as shown in Figures 7 and 8, respectively.

In the conventional triaxial compression test (Figure 10), cracks and joints develop in the sandstone, and damage occurs at the beginning of loading, but the damage is limited because of the low loading stress. Then, as the strain increases, the damage in the specimens grows at a gradually increasing rate. The growth curve changes from linear to nonlinear. When the rock sample fails and becomes unstable, the damage curve increases rapidly.

Comparing the damage curves of sandstone under different confining pressures in conventional triaxial loading tests, Figure 10 shows that, for low confining pressures, the damage increases steadily during the test, and although the growth rate becomes higher as the peak stress is approached, no sudden increase phenomenon occurs when the confining pressure is relatively high. This result indicates that the confining pressure prevents the fractures in sandstone from developing, which induces a low damage value until the specimen nears the peak stress, when increasingly more cracks appear, develop, gather, and form a macroscopic fracture surface, causing the damage to increase immediately.

According to the damage evolution of the triaxial unloading of the confining pressure (Figure 11), during the early stages of the test, the damage to sandstone is limited, and the dissipation energy is very low because of the large number of primary microcracks. With increasing axial stress, the microcracks in the sandstone begin to expand, and new cracks appear, which induces an increase in dissipation energy and damage. When the unloading stage starts, a large number of cracks in the sandstone begin to expand and converge. Moreover, a large number of new larger cracks appear continuously, and the dissipation energy of and the damage to the specimen increase rapidly. When the specimen fails, the dissipation energy increases suddenly, and the damage shows the same tendency. The sandstone then enters the plastic flow stage in which the dissipation energy is reduced and the damage tends to be relatively stable.

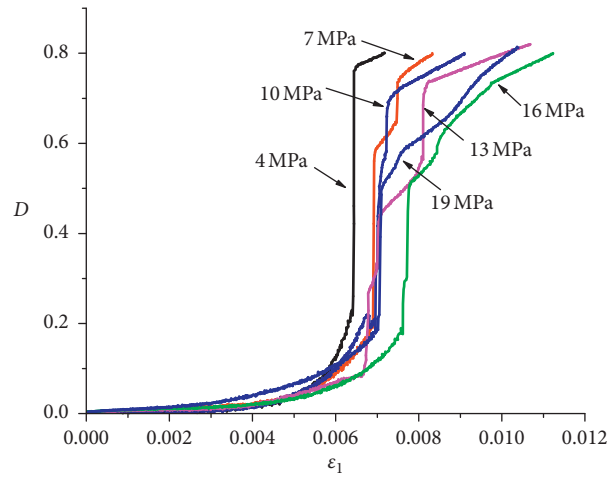

Figure 10: Damage curves of rock samples under conventional triaxial compression based on the dissipation energy.

Comparing the damage to sandstone during conventional triaxial compression tests and triaxial unloading confining pressure tests, the sudden increase in the damage to the sandstone near the peak stress is more obvious in the latter tests because of the unloading effect of the confining pressure.

7. Discussion

The energy evolution characteristics of sandstone samples under different confining pressures are studied in this paper, and some differences in the scale and mechanical properties are found between rock samples and actual rock masses. Studying the energy evolution law of rock samples during unloading confining pressure failure can further clarify the energy characteristics of the unloading confining pressure failure of rock samples. The greater the burial depth, the more the energy stored in the rock mass. Inducing a sudden release of a large amount of energy during excavation is easy. Therefore, during the process of deep rock mass excavation, some engineering measures should be taken to release internal energy in a timely manner. Although the research results cannot be directly used in field engineering, the principles revealed by the results are similar to those of unloading failure during the actual rock excavation process. Further applying these principles in engineering is the direction of follow-up research.

8. Conclusions

In this study, we conducted conventional triaxial compressional loading tests and triaxial unloading confining pressure tests under different loading paths for sandstone specimens. The results show that more energy is stored and consumed before the stress reaches its peak, while after the peak stress, more energy is released and consumed. The energy dissipation causes the internal cracks in the sandstone to expand, resulting in damage and deterioration, and the released energy causes the failure of the sandstone.

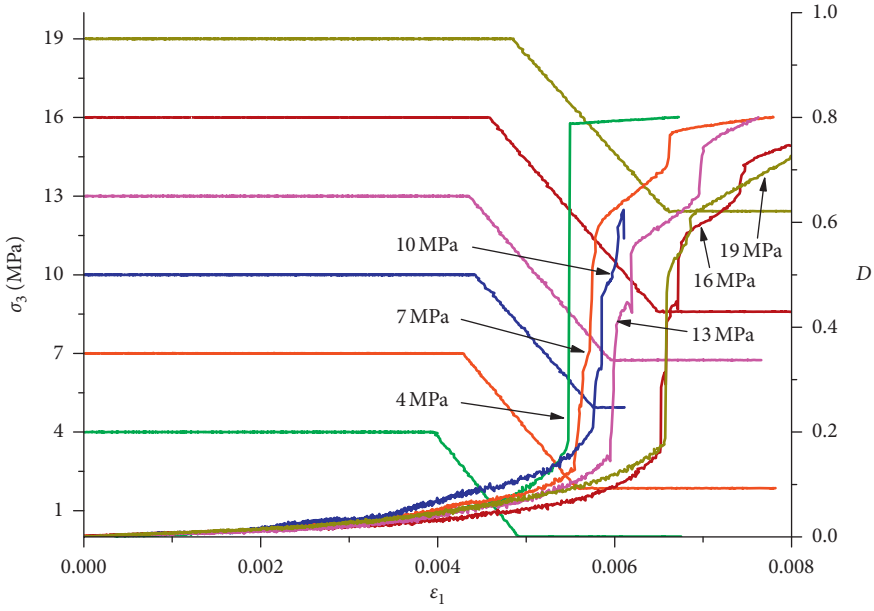

Figure 11: Damage curves of rock samples under unloading of the confining pressure based on the dissipation energy.

In the triaxial unloading confining pressure tests, the higher the initial confining pressure, the more the elastic energy stored in the sandstone; thus, under higher confining pressures, more energy is released when the failure of sandstone occurs, resulting in more severe disasters. In actual engineering, the release of elastic energy in rock under high-stress conditions is significantly higher than that in rock under low-stress conditions when the rock fails. Therefore, when a high-stress rock mass is excavated, much elastic energy can be released rapidly, resulting in rock burst and other geological disasters.

The higher the initial confining pressure, the more the energy consumed when the radial deformation does work to overcome the confining pressure during the axial loading stage. The dissipation energy also increases with the initial confining pressure caused by the appearance and development of cracks. This result demonstrates that the initial confining pressure has a great influence on the radial deformation of sandstone samples.

Compared to conventional triaxial compression tests, triaxial unloading confining pressure tests cause more obvious changes in the rock damage when the failure of sandstone occurs, and the unloading effect of the confining pressure contributes to this phenomenon. The rock failure caused by unloading is also concluded to be more serious than that caused by loading.

Data Availability

The data used to support the findings of this study are available from the corresponding author upon request.

Conflicts of Interest

The authors declare that there are no conflicts of interest related to the publication of this paper.

Acknowledgments

This study was supported by the National Key R&D Program of China (2018YFC0604705), the National Natural Science Foundation of China (51574156), and the Shandong Province Higher Educational Science and Technology Program (J18KA195).

References

[1] L. Du, Y. P. Wang, and D. Z. Ming, "Numerical analysis of influence of pit unloading on underlying metro tunnel," *Journal of Shandong University of Science and Technology (Natural Science)*, vol. 35, no. 6, pp. 62–67, 2006.

[2] T. W. Lan, H. W. Zhang, J. Han, W. H. Song, H. Wu, and Z. C. Cai, "Study on rock burst mechanism based on geostress and energy principle," *Journal of Mining and Safety Engineering*, vol. 29, no. 6, pp. 840–875, 2012.

[3] Y. Cong, Z. Q. Wang, Y. R. Zheng, X. T. Feng, and L. M. Zhang, "Energy evolution principle of fracture propagation of marble with different unloading stress paths," *Journal of Central South University (Science and Technology)*, vol. 47, no. 9, pp. 3140–3147, 2016.

[4] S. Q. Yang, W. Y. Xun, and C. D. Su, "Study on the deformation failure and energy properties of marble specimen under triaxial compression," *Engineering Mechanics*, vol. 24, no. 1, pp. 136–142, 2007.

[5] T. W. Liu, J. D. He, and W. J. Xu, "Energy properties of failure of marble samples under triaxial compression," *Chinese Journal of Geotechnical Engineering*, vol. 35, no. 2, pp. 395–400, 2013.

[6] W. Z. Chen, S. P. Lv, X. H. Guo, and C. J. Qiao, "Research on unloading confining pressure tests and rock burst criterion based on energy theory," *Chinese Journal of Rock Mechanics and Engineering*, vol. 28, no. 8, pp. 1530–1540, 2009.

[7] X. Z. Chen, J. D. He, H. Q. Xie, M. L. Xiao, and J. F. Liu, "Study on deformation failure and energy properties of marble under unloading and high confining pressure," *Journal of Sichuan*

University (Engineering Science Edition), vol. 46, no. S2, pp. 60–64, 2014.

[8] F. J. Zhao, H. Y. Wang, Y. Peng, and G. J. Wang, "Experimental research on acoustic emission energy and rock crushing effect under static-dynamic coupling loading," *Chinese Journal of Rock Mechanics and Engineering*, vol. 31, no. 7, pp. 1363–1368, 2012.

[9] D. Huang, R. Q. Huang, and Y. X. Zhang, "Experimental investigations on static loading rate effects on mechanical properties and energy mechanism of coarse crystal grain marble under uniaxial compression," *Chinese Journal of Rock Mechanics and Engineering*, vol. 31, no. 2, pp. 245–255, 2012.

[10] Y. Pan, Z. Q. Wang, and A. W. Li, "Comprehensive rigidity and comprehensive energy criterion of the rock burst," *Rock and Soil Mechanics*, vol. 30, no. 12, pp. 3671–3676, 2009.

[11] Y. M. Song and X. B. Yang, "Evolution characteristics of deformation and energy fields during coal pillar instability," *Journal of Mining and Safety Engineering*, vol. 30, no. 6, pp. 822–827, 2013.

[12] H. Zhang, L. X. Cheng, and G. S. Li, "Study of energy dissipation characteristics of saturated coal sample based on Brazil splitting method," *Journal of Experimental Mechanics*, vol. 31, no. 4, pp. 534–542, 2016.

[13] Z. Q. Ma, Y. D. Jiang, Y. W. Li, Y. M. Yang, and H. T. Li, "Experimental research on influence of loading rate and confining pressure on energy evolution of coal," *Chinese Journal of Geotechnical Engineering*, vol. 38, no. 11, pp. 2114–2121, 2016.

[14] L. Meng, T. Li, A. Liao, and P. Zeng, "Anisotropic mechanical properties of sandstone under unloading confining pressure at high temperatures," *Arabian Journal for Science and Engineering*, vol. 43, no. 10, pp. 5283–5294, 2018.

[15] D. Yang, D. Zhang, S. Niu, Y. Dang, W. Feng, and S. Ge, "Experiment and study on mechanical property of sandstone post-peak under the cyclic loading and unloading," *Geotechnical and Geological Engineering*, vol. 36, no. 3, pp. 1609–1620, 2018.

[16] D.-M. Zhang, Y.-Z. Yang, Y.-P. Chu, X. Zhang, and Y.-G. Xue, "Influence of loading and unloading velocity of confining pressure on strength and permeability characteristics of crystalline sandstone," *Results in Physics*, vol. 9, pp. 1363–1370, 2018.

[17] Q. Meng, M. Zhang, L. Han, H. Pu, and Y. Chen, "Acoustic emission characteristics of red sandstone specimens under uniaxial cyclic loading and unloading compression," *Rock Mechanics and Rock Engineering*, vol. 51, no. 4, pp. 969–988, 2018.

[18] H. L. Wang, W. Y. Xu, M. Cai, Z. P. Xiang, and Q. Kong, "Gas permeability and porosity evolution of a porous sandstone under repeated loading and unloading conditions," *Rock Mechanics and Rock Engineering*, vol. 50, no. 8, pp. 2071–2083, 2017.

[19] Q.-L. Ding, F. Ju, X.-B. Mao, D. Ma, B.-Y. Yu, and S.-B. Song, "Experimental investigation of the mechanical behavior in unloading conditions of sandstone after high-temperature treatment," *Rock Mechanics and Rock Engineering*, vol. 49, no. 7, pp. 2641–2653, 2016.

[20] H. P. Xie, R. D. Peng, and Y. Ju, "Energy dissipation of rock deformation and fracture," *Chinese Journal of Rock Mechanics and Engineering*, vol. 23, no. 21, pp. 3565–3570, 2004.

[21] M. Li, J. X. Zhang, N. Zhou, and Y. L. Huang, "Effect of particle size on the energy evolution of crushed waste rock in coal mines," *Rock Mechanics and Rock Engineering*, vol. 50, no. 5, pp. 1347–1354, 2017.

[22] Q. Meng, M. Zhang, L. Han, H. Pu, and T. Nie, "Effects of acoustic emission and energy evolution of rock specimens under the uniaxial cyclic loading and unloading compression," *Rock Mechanics and Rock Engineering*, vol. 49, no. 10, pp. 3873–3886, 2016.

[23] D. Y. Li, Z. Sun, T. Xie, X. B. Li, and P. G. Ranjith, "Energy evolution characteristics of hard rock during triaxial failure with different loading and unloading paths," *Engineering Geology*, vol. 228, pp. 270–281, 2017.

[24] L. M. Kachanov, "Rupture Time Under Creep Conditions," *International Journal of Fracture*, vol. 97, pp. 11–18, 1999.

[25] B. X. Liu, J. L. Huang, Z. Y. Wang, and L. Liu, "Study on damage evolution and acoustic emission character of coal-rock under uniaxial compression," *Chinese Journal of Rock Mechanics and Engineering*, vol. 28, no. S1, pp. 3234–3238, 2009.